Speed Control of the Surface-Mounted Permanent-Magnet Synchronous Motor Based on Takagi–Sugeno Fuzzy Models

Yuan-Chih Chang, *Member, IEEE*, Chien-Hua Chen, Zhong-Chuan Zhu, and Yi-Wen Huang

***Abstract*—The speed control of the surface-mounted permanent-magnet synchronous motor (SPMSM) based on Takagi–Sugeno (T–S) fuzzy models is designed and implemented in this paper. In motor drive speed control, proportional-integral controller is generally applied. However, the tracking performance and load regulation capability should be compromised in the designing process of the controller. This study develops a speed controller based on the T–S fuzzy model with good tracking ability and load variation regulation. First, the dynamic model of an SPMSM is demonstrated and the load torque variation is treated as disturbances. Accordingly, the speed control strategy is developed based on the T–S fuzzy model. The defuzzification process and parallel distributed compensation are introduced. The ability of disturbance suppression and the Lyapunov stability of this system are established and analyzed. The controller gains are obtained via the linear matrix inequality toolbox. The speed control and all essential procedures are realized by the microcontroller Renesas RX62T. The tracking performance and load regulation capability are verified by the experimental results.**

***Index Terms*—Linear matrix inequality, permanent-magnet synchronous motor, speed control, T–S fuzzy.**

I. Introduction

PERMANENT-MAGNET synchronous motors (PMSM) [1] can be widely found in the applications of electric vehicles (EV) [2]–[4], hybrid electric vehicles [4], elevators [5], wind energy conversion systems [6], compressors [7], and flywheel energy storage systems (FESS) [8]. The merits of a PMSM include high-power density, robust structure, low maintenance cost, and high conversion efficiency. The categories of a PMSM can be divided into surface-mounted PMSM (SPMSM) [9] and interior PMSM (IPMSM) [10], [11] according to the embedding type of its permanent magnet. For the application of low-torque ripple, an SPMSM is adopted. For higher torque generating capability, an IPMSM is generally selected. Magnet designs [12], [13] of the PMSM are also proposed to minimize the torque ripple and optimize the performance.

Dynamic control is essential to obtain good driving performance of a PMSM. In the literatures, current control [14], direct torque control [15], and speed control [16] are implemented according to the objective of a PMSM drive. With the advancement of a modern control theory, many nonlinear control techniques are proposed to deal with the nonlinearity of the PMSM drive system. For example, adaptive control [17] is proposed to control the speed of a PMSM with load inertia variation. Sliding mode control [18] is utilized in designing an observer to estimate the velocity and load of an SPMSM. The designed sliding mode controller yield better performance when the sampling period is increased. Robust control [19] with speed estimator is developed to achieve good speed trajectory tracking performance under the presence of disturbances. The fuzzy logic controller [20] is combined with the proportional-integral controller to obtain good performance under both transient and steady-state conditions. Internal model control [21] with fuzzy adaptive law is designed to automatically tune the parameter of speed controller. Furthermore, to deal with the uncertainties and disturbances, fuzzy neural network [22], disturbance observer feedforward compensation [23], and high-gain observer [24] are proposed to enhance the performance of the controller. In recent years, the Takagi–Sugeno fuzzy [25] (T–S fuzzy) is also implemented in the PMSM drive system. However, large load torque variations of the PMSM are not treated. The speed control developed in this paper is designed based on the T–S fuzzy models to deal with a large load torque variation. The load torque variation is considered as disturbances of the PMSM drive system. In traditional PID control, the controller parameters should be adjusted according to the variations of system parameters. With the proposed control, good tracking and regulation capabilities can be obtained without adjusting any controller parameter. The power rating of the established PMSM drive is 4.5 kW, which is suitable for the applications of EV, FESS, and compressors.

In this paper, the system configuration of the developed SPMSM drive is first introduced. Next, the nonlinear dynamic models of the SPMSM are demonstrated. The speed controller is designed based on T–S fuzzy models of an SPMSM and the load torque variation is considered as disturbances. Furthermore, the nonlinear system of the SPMSM is approximated into several linear subsystems via the IF–THEN rules. The controller gains of the linear subsystems are designed by using a parallel distributed compensation (PDC). The stability of the proposed speed controller is proved via Lyapunov theorem. Finally, the controller gains are obtained by the linear matrix inequality (LMI) toolbox. The tracking performance and the speed regulation under large torque variation are verified by the experimental results.

Manuscript received October 1, 2015; accepted November 18, 2015. Date of publication November 30, 2015; date of current version March 25, 2016. This work was supported in part by the Ministry of Science and Technology, Taiwan, under Grant of MOST 104-2221-E-194-016. Recommended for publication by Associate Editor B. Wang.

The authors are with the Advanced Institute of Manufacturing with High-tech Innovations, Department of Electrical Engineering, National Chung Cheng University, Chiayi, Taiwan 62102 (e-mail: ycchang@ccu.edu.tw; tony22288@hotmail.com; zxc221108@gmail.com; candy4122@yahoo.com.tw).

Color versions of one or more of the figures in this paper are available online at http://ieeexplore.ieee.org.

Digital Object Identifier 10.1109/TPEL.2015.2504392

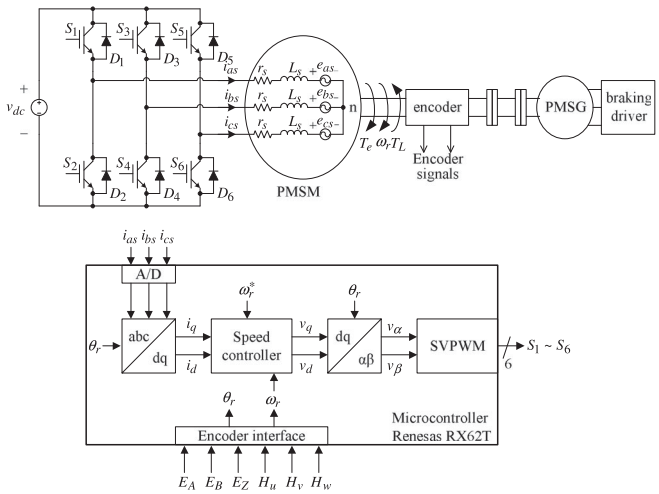

Fig. 1. System configuration of the developed SPMSM drive system.

II. System Configuration and Dynamic Models

Fig. 1 shows the system configuration of the developed SPMSM drive system. A permanent-magnet synchronous generator with braking driver is served as the source of load torque. The variation of load torque can be adjusted by the braking driver. Three-phase winding currents and encoder signals are sensed and properly filtered. The encoder signals are used to calculate the rotor speed and position. The feedback current signals are transformed to rotor reference frame (*dq*-frame). The rotor speed command, actual rotor speed, and *dq*-frame currents are implemented in the proposed speed control algorithm. The control efforts (v_q, v_d) generated by the speed controller are transformed to stationary reference frame. The duty ratios of the six power switches are determined by space-vector pulse-width modulation. All the control and transformation schemes are digitally realized by the microcontroller Renesas RX62T.

The voltage equations of an SPMSM expressed in rotor reference frame can be written as

$$\begin{aligned} v_q &= r_s i_q + L_q \dot{i}_q + \omega_r L_d i_d + \omega_r \lambda_m \\ v_d &= r_s i_d + L_d \dot{i}_d - \omega_r L_q i_q \end{aligned} \tag{1}$$

where v_q and v_d are *dq*-frame voltages, i_q and i_d are *dq*-frame currents, r_s is winding resistance, L_q and L_d are *dq*-frame inductances, ω_r is electrical rotor speed, and λ_m is flux linkage established by the permanent magnet.

The mechanical equation of a SPMSM is

$$T_e = J\left(\frac{2}{P}\right)\dot{\omega}_r + B\left(\frac{2}{P}\right)\omega_r + T_L \tag{2}$$

where T_e is the electromagnetic torque generated by SPMSM, *J* is the inertia of SPMSM system, *B* is the damping coefficient of SPMSM system, T_L is the load torque, and *P* is the number of magnetic poles.

Moreover, the electromagnetic torque generated by an SPMSM is

$$T_e = \left(\frac{3}{2}\right)\left(\frac{P}{2}\right)\left[\lambda_m i_q + (L_q - L_d) i_q i_d\right]. \tag{3}$$

For the SPMSM, *q*-axis inductance is close to *d*-axis inductance $(L_q \cong L_d)$. The electromagnetic torque in (3) can be simplified as

$$T_e = \left(\frac{3}{2}\right)\left(\frac{P}{2}\right)\lambda_m i_q. \tag{4}$$

The state equations of the SPMSM can be obtained by summarizing (1)–(4)

$$\begin{aligned} \dot{i}_q &= \frac{1}{L_q}\left(v_q - r_s i_q - \omega_r L_d i_d - \omega_r \lambda_m\right) \\ \dot{i}_d &= \frac{1}{L_d}\left(v_d - r_s i_d + \omega_r L_q i_q\right) \\ \dot{\omega}_r &= \frac{1}{J}\left[\left(\frac{P}{2}\right)(T_e - T_L) - B\omega_r\right] \\ &= \left(\frac{3P^2}{8J}\lambda_m i_q - \frac{B}{J}\omega_r - \frac{P}{2J}T_L\right). \end{aligned} \tag{5}$$

It is obvious that the state equations of an SPMSM are nonlinear. The speed controller based on T–S fuzzy models will be derived via these equations.

III. Design of Speed Controller Based on T–S Fuzzy Models

In the T–S fuzzy models, the nonlinear system of an SPMSM is represented by several linear subsystems according to the model rules

$$\begin{aligned} &\text{Model rules } i: \\ &If\ z_1(t)\ \text{is}\ M_{\text{il}}\ \text{and}\ \ldots\ \text{and}\ z_p(t)\ \text{is}\ M_{\text{ip}} \\ &\text{then}\ \dot{x}(t) = A_i x(t) + B_i u(t) \end{aligned} \tag{6}$$

where M_{ip} is the fuzzy set, *x*(*t*) are the state variables, *u*(*t*) are the control inputs, A_i, B_i are the state matrices of the subsystem, and ω_r will be selected as $z_p(t)$ to represent the nonlinear system. After defuzzification, the fuzzy system of an SPMSM can be expressed as

$$\dot{x}(t) = \sum_{i=1}^{r} h_i\left(z(t)\right)\left\{A_i x(t) + B_i u(t)\right\} \tag{7}$$

where

$$h_i(z(t)) = \frac{\prod_{j=1}^{r} M_{ij}\left(z_j(t)\right)}{\sum_{i=1}^{r}\prod_{j=1}^{r} M_{ij}\left(z_j(t)\right)} \tag{8}$$

and $M_{ij}(z_j(t))$ is the grad of membership.

The PDC controllers corresponding to the model rules can be expressed as

$$\begin{aligned} &\text{Control rules } i: If\ Z_1(t)\ \text{is}\ M_{\text{i}}1\ \text{and}\ \ldots\ \text{and}\ z_p(t)\ \text{is}\ M_{\text{ip}} \\ &\text{then}\ u(t) = -\sum_{i=1}^{r} h_i\left(z(t)\right) K_i x(t). \end{aligned} \tag{9}$$

The close-loop system can be obtained by substituting (9) into (6)

$$\dot{x}(t) = \sum_{i=1}^{r}\sum_{i=1}^{r} h_j\left(z(t)\right) h_j\left(z(t)\right)\left\{A_i - B_i K_j\right\} x(t) \tag{10}$$

To ensure the tracking capability of the speed controller, a new state variable is defined

$$x_e(t) = \int [r(t) - y(t)]\, dt \tag{11}$$

where

$$y(t) = \omega_r \tag{12}$$

and $r(t)$ is the desired value of ω_r.

By combing (5) and (11), the state equations of a SPMSM are

$$\begin{bmatrix} \dot{\omega}_r \\ \dot{i}_q \\ \dot{i}_d \\ \dot{x}_e \end{bmatrix} = \begin{bmatrix} -\frac{B}{J} & \frac{3P^2\lambda_m}{8J} & 0 & 0 \\ -\frac{\lambda_m}{L_q} & -\frac{r_s}{L_q} & -\frac{L_d}{L_q}\omega_r & 0 \\ 0 & \frac{L_q}{L_d}\omega_r & -\frac{r_s}{L_d} & 0 \\ -1 & 0 & 0 & 0 \end{bmatrix} \begin{bmatrix} \omega_r \\ i_q \\ i_d \\ x_e \end{bmatrix} + \begin{bmatrix} 0 & 0 \\ \frac{1}{L_q} & 0 \\ 0 & \frac{1}{L_d} \\ 0 & 0 \end{bmatrix} \begin{bmatrix} v_q \\ v_d \end{bmatrix} + \begin{bmatrix} -\frac{PT_L}{2J} \\ 0 \\ 0 \\ r \end{bmatrix} \tag{13}$$

$$\begin{aligned} \dot{x}(t) &= Ax(t) + Bu(t) + \eta(t) \\ y(t) &= \begin{bmatrix} 1 & 0 & 0 & 0 \end{bmatrix} x(t) = Cx(t) \end{aligned} \tag{14}$$

where $\eta(t)$ are disturbances of the system.

For convenience, the disturbances are further represented by

$$\eta(t) = \begin{bmatrix} -\frac{PT_L}{2J} \\ 0 \\ 0 \\ r \end{bmatrix} = \begin{bmatrix} -\frac{P}{2J} & 0 & 0 & 0 \\ 0 & 0 & 0 & 0 \\ 0 & 0 & 0 & 0 \\ 0 & 0 & 0 & 1 \end{bmatrix} \begin{bmatrix} T_L \\ 0 \\ 0 \\ r \end{bmatrix} = Ev(t) \tag{15}$$

where $v(t)$ are the disturbance signals of the system.

The state equations in (14) are rewritten as

$$\dot{x}(t) = Ax(t) + Bu(t) + Ev(t). \tag{16}$$

The rated speed ω_r of the developed SPMSM drive system is 753.98 rad/s. The membership functions of ω_r are demonstrated in Fig. 2(a). N is the membership function of rule 1, $\bar{N}$ is the membership function of rule 2, d is the minimum value of ω_r, and D is the maximum value of ω_r. The membership functions can be represented as

$$N = \frac{1}{D-d}\omega_r + \frac{-d}{D-d},\ \bar{N} = 1 - N. \tag{17}$$

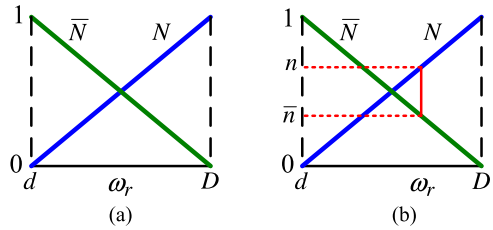

Fig. 2. (a) Membership functions of ω_r, (b) weighting of the membership functions.

For a particular value of ω_r, the weightings of the membership functions can be found

$$w_1 = n, \quad w_2 = \bar{n} \tag{18}$$

$$H = \sum_{i=1}^{2} w_i, \quad h_i = \frac{w_i}{H} \tag{19}$$

where w_1 is the grade of the membership function N and w_2 is the grade of the membership function $\bar{N}$. The controller gain K_i in (9) and the weightings h_i in (19) are used in the close-loop speed controller to control the speed of the SPMSM.

IV. System Stability Analysis

According to the state equations expressed in (16), the SPMSM system based on T–S fuzzy models with disturbances can be obtained

$$\begin{aligned} \dot{x}(t) &= \sum_{i=1}^{r} h_i(z(t)) \{A_i x(t) + B_i u(t) + E_i v(t)\} \\ y(t) &= \sum_{i=1}^{r} h_i(z(t)) C_i x(t). \end{aligned} \tag{20}$$

Define the H_∞ performance index

$$\sup_{\|v(t)\|_2 \neq 0} \frac{\|y(t)\|_2}{\|v(t)\|_2} \leq \gamma, \quad 0 \leq \gamma \leq 1 \tag{21}$$

where γ represents the ability of disturbance suppression of the SPMSM drive system.

Lemma: Assume that there is a positive definite matrix $P = X^{-1}$, which makes the following LMI condition be feasible: [see (22) shown at the bottom of the next page], where

$$X > 0, M = KX, i < js.t. h_i(z(t)) \cap h_j(z(t)) \neq \varphi. \tag{23}$$

Then, the designed speed controller

$$u(t) = \sum_{i=1}^{r} h_i(z(t)) K_i x(t) \tag{24}$$

can ensure the speed tracking error converge to zero.

Proof: Assume that there is a quadratic form function $V(x(t)) = x^T(t) \cdot P \cdot x(t)$, $P = X^{-1} > 0$ and $\gamma > 0$ for all time t, then the LMI condition is

$$\dot{V}(x(t)) + y^T(t)y(t) - \gamma^2 v^T(t)v(t) \leq 0. \tag{25}$$

Properly and carefully substituting (20) and (24) into (25)

$$\begin{aligned}&\dot{x}^T(t)Px(t)+x^T(x)P\dot{x}(t)+y^T(t)y(t)-\gamma^2v^T(t)v(t)\\&=\sum_{i=1}^{r}h_i(z(t))\left\{A_ix(t)+B_iu(t)+E_iv(t)\right\}^T Px(t)\\&+x^T(x)P\sum_{i=1}^{r}h_i(z(t))\left\{A_ix(t)+B_iu(t)+E_iv(t)\right\}\\&+\sum_{i=1}^{r}\sum_{j=1}^{r}h_i(z(t))h_j(z(t))x^T(t)C_i^TC_jx(t)-\gamma^2v^T(t)v(t)\\&=\sum_{i=1}^{r}\sum_{j=1}^{r}h_i(z(t))h_j(z(t))\begin{bmatrix}x^T(t) & v^T(t)\end{bmatrix}\\&\begin{bmatrix}(A_i-B_iK_j)^TP & \\ +P(A_i-B_iK_j) & PE_i\\ +C_i^TC_j & \\ E_i^TP & -\gamma^2I\end{bmatrix}\begin{bmatrix}x(t)\\ v(t)\end{bmatrix}.\end{aligned}\tag{26}$$

By using (26), the LMI condition in (25) is expressed as

Equation (27) shown at the bottom of the page can be rewritten as:

$$\begin{bmatrix}-\sum_{i=1}^{r}\sum_{j=1}^{r}h_i(z(t))h_j(z(t))[(A_i-B_iK_j)^TP & \\ +P(A_i-B_iK_j)] & -P\sum_{i=1}^{r}h_i(z(t))E_i\\ -\sum_{i=1}^{r}h_i(z(t))E_i^TP & \gamma^2I\end{bmatrix}$$

$$-\begin{bmatrix}\sum_{i=1}^{r}h_i(z(t))C_i^T\\ 0\end{bmatrix}\begin{bmatrix}\sum_{i=1}^{r}h_i(z(t))C_i & 0\end{bmatrix}\geq 0.\tag{28}$$

Applying the Schur Complement

$$A-B^TCB<0\Leftrightarrow\begin{bmatrix}A & B^T\\ B & C\end{bmatrix}<0.\tag{29}$$

TABLE I
MOTOR PARAMETERS OF THE SPMSM

poles	R_s	$L_d \cong L_q$	Back EMF constant	rated speed	rated torque	rated power
8	0.24 Ω	2.014 mH	99.79 V/k·r/min	1800 r/min	23 N·m	4.5 kW

Then, (28) is rewritten as (30) shown at bottom of the next page

For convenience, the LMI condition (30) shown at bottom of the next page is expressed as (31) shown at bottom of the next page

According to (31) shown at bottom of the next page, the new LMI condition becomes

If the LMI in (32) shown at bottom of the next page are multiplied on both sides of the matrix with

$$\begin{bmatrix}X & 0 & 0\\ 0 & I & 0\\ 0 & 0 & I\end{bmatrix}.\tag{33}$$

The LMI condition shown in (22) is obtained.

By using the LMI condition in (22) and let $\gamma=0.8$, the following controller gains are obtained

$$K_1=\begin{bmatrix}-0.00425 & 0.00246 & 0.00811 & -2.596\\ 0.00495 & -0.00281 & 0.0024 & -0.1602\end{bmatrix}$$

$$K_2=\begin{bmatrix}-0.00475 & 0.00246 & 0.00811 & -2.616\\ 0.00515 & -0.00081 & 0.0004 & -0.1582\end{bmatrix}.\tag{34}$$

V. EXPERIMENTAL RESULTS

The experimental setup of the developed SPMSM drive system is shown in Fig. 3. The motor parameters are listed in Table I. The specifications of the SPMSM drive are shown in Table II.

$$\begin{bmatrix}\left(-\frac{1}{2}\begin{pmatrix}A_iX-B_iM_j+XA_i^T-M_j^TB_i^T\\ +A_jX-B_jM_i+XA_j^T-M_i^TB_j^T\end{pmatrix}\right) & -\frac{1}{2}(E_i+E_j) & -\frac{1}{2}X(C_i+C_j)^T\\ -\frac{1}{2}(E_i+E_j)^T & \gamma^2I & 0\\ \frac{1}{2}(C_i+C_j)X & 0 & I\end{bmatrix}\geq 0\tag{22}$$

$$\begin{bmatrix}-\sum_{i=1}^{r}\sum_{j=1}^{r}h_i(z(t))h_j(z(t))[(A_i-B_iK_j)^TP & \\ +P(A_i-B_iK_j)+C_i^TC_j] & -P\sum_{i=1}^{r}h_i(z(t))E_i\\ -\sum_{i=1}^{r}h_i(z(t))E_i^TP & \gamma^2I\end{bmatrix}\geq 0\tag{27}$$

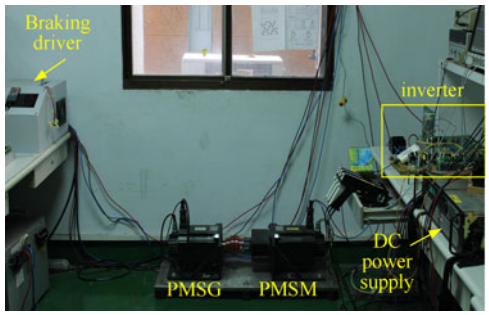

Fig. 3. Experimental setup of the developed SPMSM drive system.

TABLE II
SPECIFICATIONS OF THE SPMSM DRIVE

Rated power	5 kW	DC-link voltage	$380V_{dc}$
rated voltage	$220V_{rms}$	Dc-link capacitance	5600 μF
rated current	$13.1A_{rms}$	switching frequency	20 kHz

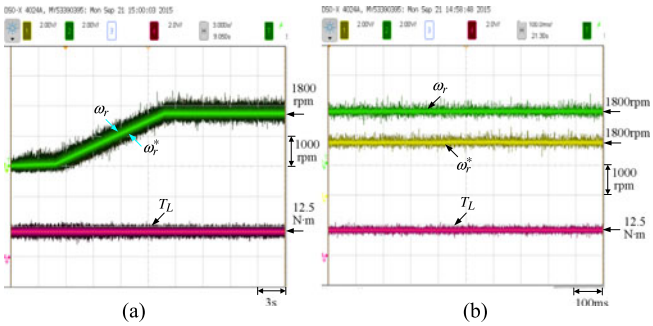

Fig. 4. Starting from stall at $T_L = 12.5$ N·m: (a) full waveforms of $(\omega_r, \omega_r^*, T_L)$, (b) expansion waveforms of $(\omega_r, \omega_r^*, T_L)$.

A. Starting From Stall

The measured waveforms of the SPMSM starting from stall at half-rated load torque (12.5 N·m) and rated load torque (23 N·m) are shown in Figs. 4 and 5, respectively. It is obvious that the SPMSM can be successfully started from stall to rated speed at different load torque conditions.

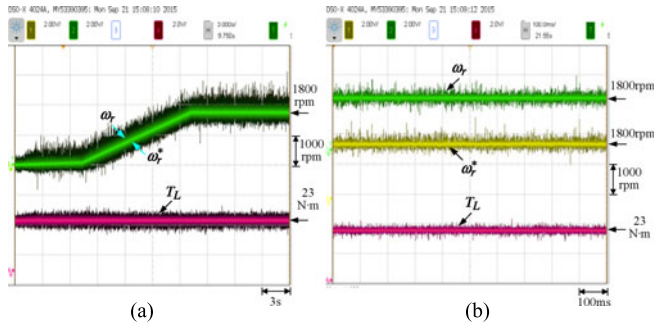

Fig. 5. Starting from stall at $T_L = 23$ N·m: (a) full waveforms of $(\omega_r, \omega_r^*, T_L)$, (b) expansion waveforms of $(\omega_r, \omega_r^*, T_L)$.

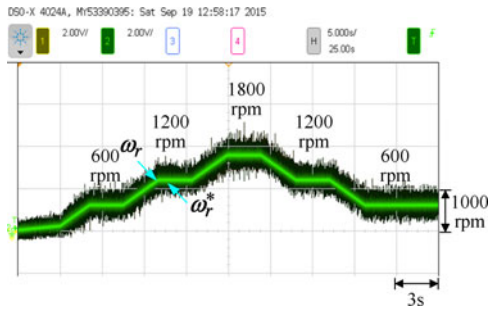

Fig. 6. Speed command tracking waveforms of the SPMSM from 600 r/min→ 1200 r/min→ 1800 r/min→ 1200 r/min→ 600 r/min.

B. Speed Command Tracking

Fig. 6 shows the speed command tracking waveforms of the SPMSM from 600 r/min→ 1200 r/min→ 1800 r/min→ 1200 r/min→ 600 r/min. Fig. 7(a) and (b) shows the speed command tracking waveforms of the SPMSM from 900 r/min→ 1000 r/min→ 900 r/min at $T_L = 23$ N·m and $T_L = 15.3$ N·m, respectively. It can be observed that the SPMSM speed can

$$\begin{bmatrix} -\sum_{i=1}^{r}\sum_{j=1}^{r} h_i(z)h_j(z)[(A_i - B_iK_j)^T P + P(A_i - B_iK_j)] & -P\sum_{i=1}^{r} h_i(z)E_i & \sum_{i=1}^{r} h_i(z)C_i^T \\ -\sum_{i=1}^{r} h_i(z)E_i^T P & \gamma^2 I & 0 \\ \sum_{i=1}^{r} h_i(z)C_i & 0 & I \end{bmatrix} \geq 0 \tag{30}$$

$$\sum_{i=1}^{r}\sum_{j=1}^{r} h_i(z)h_j(z) \begin{bmatrix} -\frac{1}{2}\left\{ \begin{matrix} (A_i - B_iK_j)^T P + P(A_i - B_iK_j) \\ +(A_j - B_jK_i)^T P + P(A_j - B_jK_i) \end{matrix} \right\} & -\frac{1}{2}P(E_i + E_j) & -\frac{1}{2}(C_i + C_j)^T \\ -\frac{1}{2}(E_i + E_j)^T P & \gamma^2 I & 0 \\ \frac{1}{2}(C_i + C_j) & 0 & I \end{bmatrix} \geq 0. \tag{31}$$

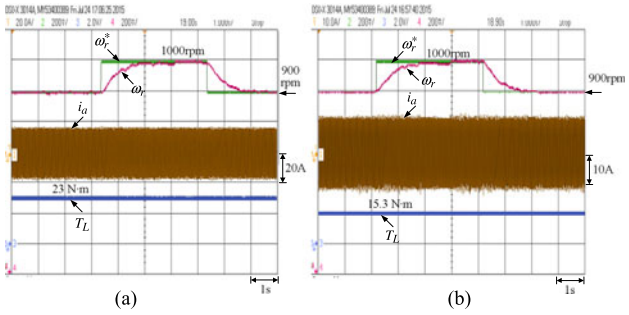

Fig. 7. Speed command tracking waveforms of the SPMSM from 900 r/min→ 1000 r/min→ 900 r/min: (a) at $T_L = 23$ N·m, (b) at $T_L = 15.3$ N·m.

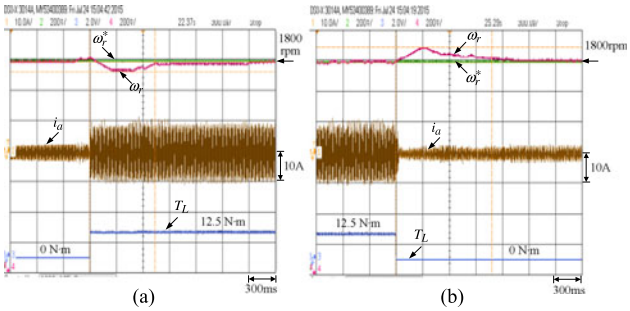

Fig. 8. Speed regulation under load torque variations at $\omega_r = 1800$ r/min: (a) $T_L = 0 \rightarrow 12.5$ N·m, (b) $T_L = 12.5 \rightarrow 0$ N·m.

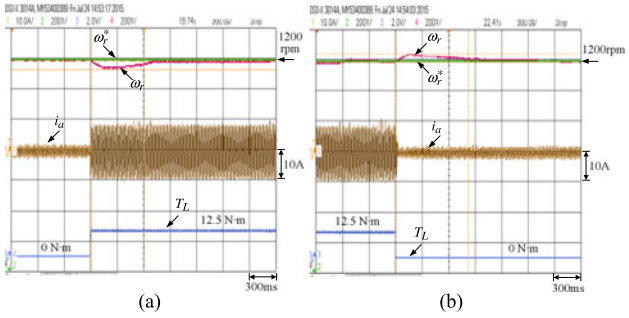

Fig. 9. Speed regulation under load torque variations at $\omega_r = 1200$ r/min: (a) $T_L = 0 \rightarrow 12.5$ N·m, (b) $T_L = 12.5 \rightarrow 0$ N·m.

correctly track the speed command at different speed and load torque conditions.

C. Load Torque Regulation

To verify the dynamic performance of the proposed speed control due to load torque variation, the speed regulation

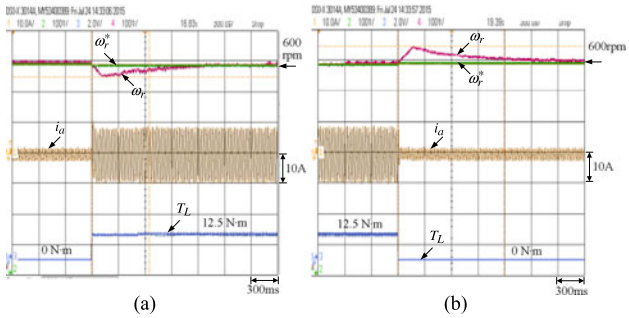

Fig. 10. Speed regulation under load torque variations at $\omega_r = 600$ r/min: (a) $T_L = 0 \rightarrow 12.5$ N·m, (b) $T_L = 12.5 \rightarrow 0$ N·m.

TABLE III
SPEED OVERSHOOT AND SPEED UNDERSHOOT OF THE SPMSM UNDER LOAD TORQUE VARIATION AT DIFFERENT SPEED CONDITIONS

	600 rpm	1200 rpm	1800 rpm
0→3.8N·m	2 rpm	3 rpm	3 rpm
3.8→0N·m	2 rpm	3 rpm	3 rpm
0→7.6N·m	2 rpm	3 rpm	3 rpm
7.6→0N·m	2 rpm	3 rpm	4 rpm
0→11.5N·m	3 rpm	3 rpm	3 rpm
11.5→0N·m	3 rpm	3 rpm	4 rpm

waveforms at different speed commands under load torque variations $T_L = 0 \rightarrow 12.5 \rightarrow 0$ N·m are shown in Figs. 8–10, respectively. It can be observed from the results that the speed is well regulated under large load torque variations. The speed overshoot and speed undershoot of the SPMSM under load torque variation at different speed conditions are listed in Table III. The speed overshoot and undershoot is less than 4 r/min at all conditions.

VI. CONCLUSION

The speed control of the SPMSM based on T–S fuzzy models is developed in this paper. The nonlinear dynamic models of the SPMSM are implemented in the design of speed controller. The system stability of the proposed speed controller is analyzed. Experimental results verify the performance of starting from stall, speed command tracking, and load torque variation. The SPMSM can be started from stall to rate at different load torque conditions. Furthermore, the speed command tracking can be achieved at various speed and load torque conditions. The speed is also well regulated under large load torque variations via the proposed speed controller. The speed overshoot and undershoot are quite small under load torque variation.

$$\begin{bmatrix} -\frac{1}{2}\left\{\begin{matrix}(A_i - B_iK_j)^T P + P(A_i - B_iK_j) \\ +(A_j - B_jK_i)^T P + P(A_j - B_jK_i)\end{matrix}\right\} & -\frac{1}{2}P(E_i + E_j) & -\frac{1}{2}(C_i + C_j)^T \\ -\frac{1}{2}(E_i + E_j)^T P & \gamma^2 I & 0 \\ \frac{1}{2}(C_i + C_j) & 0 & I \end{bmatrix} \geq 0. \tag{32}$$

REFERENCES

[1] P. C. Krause, O. Wasynczuk, and S. D. Sudhoff, *Analysis of Electric Machinery and Drive System*. New York, NY, USA: Wiley, 2013.

[2] J. Hong, H. Lee, and K. Nam, "Charging method for the secondary battery in dual-inverter drive systems for electric vehicles," *IEEE Trans. Power Electron.*, vol. 30, no. 2, pp. 909–921, Feb. 2015.

[3] G. Pellegrino, A. Vagati, P. Guglielmi, and B. Boazzo, "Performance comparison between surface-mounted and interior PM motor drives for electric vehicle applications," *IEEE Trans. Ind. Electron.*, vol. 59, no. 2, pp. 803–811, Feb. 2012.

[4] Y. S. Lai, W. T. Lee, Y. K. Lin, and J. F. Tsai, "Integrated inverter/converter circuit and control technique of motor drives with dual-mode control for EV/HEV applications," *IEEE Trans. Power Electron*., vol. 29, no. 3, pp. 1358–1365, Mar. 2014.

[5] E. Jung, H. Yoo, S. K. Sul, H. S. Choi, and Y. Y. Choi, "A nine-phase permanent-magnet motor drive system for an ultrahigh-speed elevator," *IEEE Trans. Ind. Appl*., vol. 48, no. 3, pp. 987–995, May/Jun. 2012.

[6] V. Yaramasu and B. Wu, "Predictive control of a three-level boost converter and an NPC inverter for high-power PMSG-based medium voltage wind energy conversion systems," *IEEE Trans. Power Electron.*, vol. 29, no. 10, pp. 5308–5322, Oct. 2014.

[7] K. W. Lee, S. Park, and S. Jeong, "A seamless transition control of sensorless PMSM compressor drives for improving efficiency based on a dual-mode operation," *IEEE Trans. Power Electron.*, vol. 30, no. 3, pp. 1446–1456, Mar. 2015.

[8] M. García-Gracia, M. A. Cova, M. T. Villen, and A. Uson, "Novel modular and retractable permanent magnet motor/generator for flywheel applications with reduced iron losses in stand-by mode," *IET Renew. Power Gener.*, vol. 8, no. 5, pp. 551–557, 2014.

[9] Z. Wang, K. Lu, and F. Blaabjerg, "A simple startup strategy based on current regulation for back-EMF-based sensorless control of PMSM," *IEEE Trans. Power Electron.*, vol. 27, no. 8, pp. 3817–3825, Aug. 2012.

[10] T. D. Do, S. Kwak, H. H. Choi, and J. -W. Jung, "Suboptimal control scheme design for interior permanent-magnet synchronous motors: An SDRE-Based approach," *IEEE Trans. Power Electron.*, vol. 29, no. 6, pp. 3020–3031, Jun. 2014.

[11] P. B. Reddy, A. M. El-Refaie, and K. K. Huh, "Effect of number of layers on performance of fractional-slot concentrated-windings interior permanent magnet machines," *IEEE Trans. Power Electron.*, vol. 30, no. 4, pp. 2205–2218, Apr. 2015.

[12] R. Islam, I. Husain, A. Fardoun, and K. McLaughlin, "Permanent-magnet synchronous motor magnet designs with skewing for torque tipple and cogging torque reduction," *IEEE Trans. Ind. Appl.*, vol. 45, no. 1, pp. 152–160, Jan./Feb. 2009.

[13] K. C. Kim, J. Lee, H. J. Kim, and D. H. Koo, "Multiobjective optimal design for interior permanent magnet synchronous motor," *IEEE Trans. Magn.*, vol. 45, no. 3, pp. 1780–1783, Mar. 2009.

[14] Y. C. Chang, S. Y. Wang, W. F. Dai, and H. F. Chang, "Division-summation current control and one-cycle voltage regulation of the surface-mounted permanent-magnet synchronous generator," *IEEE Trans. Power Electron.*, vol. 31, no. 2, pp. 1391–1400, Feb. 2016.

[15] Y. Inoue, S. Morimoto, and M. Sanada, "Control method suitable for direct-torque-control-based motor drive system satisfying voltage and current limitation," *IEEE Trans. Ind. Appl.*, vol. 48, no. 3, pp. 970–976, May/Jun. 2012.

[16] S. K. Tseng, C. C. Tseng, T. H. Liu, and J. L. Chen, "Wide-range adjustable speed control method for dual-motor drive system," *IET Electr. Power Appl.*, vol. 9, no. 2, pp. 107–116, 2015.

[17] S. Li and Z. Liu, "Adaptive speed control for permanent-magnet synchronous motor system with variations of load inertia," *IEEE Trans. Ind. Appl.*, vol. 56, no. 8, pp. 3050–3059, Aug. 2009.

[18] J. R. Domínguez, A. Navarrete, M. A. Meza, A. G. Loukianov, and J. Canedo, "Digital sliding-mode sensorless control for surface-mounted PMSM," *IEEE Trans. Ind. Informat.*, vol. 10, no. 1, pp. 137–151, Feb. 2014.

[19] M. L. Corradini, G. Ippoliti, S. Longhi, and G. Orlando, "A quasi-sliding mode approach for robust control and speed estimation of PM synchronous motors," *IEEE Trans. Ind. Electron.*, vol. 59, no. 2, pp. 1096–1104, Feb. 2012.

[20] A. V. Sant, K. R. Rajagopal, and N. K. Sheth, "Permanent magnet synchronous motor drive using hybrid PI speed controller with inherent and noninherent switching functions," *IEEE Trans. Magn.*, vol. 47, no. 10, pp. 4088–4091, Oct. 2011.

[21] S. Li and H. Gu, "Fuzzy adaptive internal model control schemes for PMSM speed-regulation system," *IEEE Trans. Ind. Informat.*, vol. 8, no. 4, pp. 767–779, Nov. 2012.

[22] M. Nentwig and P. Mercorelli, "Throttle valve control using an inverse local linear mode tree based on a fuzzy neural network," in *Proc. IEEE Comput. Intell. Soc.*, 2008, pp. 1–6.

[23] R. R. Chladny and C. R. Koch, "Flatness-based tracking of an eletromechanical variable valve timing actuator with disturbance observer feedforward compensation," *IEEE Trans. Control Syst. Technol.*, vol. 16, no. 4, pp. 652–663, Jul. 2008.

[24] P. Mercorelli, "A two-stage sliding-mode high-gain observer to reduce uncertainties and disturbances effects for sensorless control in automotive applications," *IEEE Trans. Ind. Electron.*, vol. 62, no. 9, pp. 5929–5940, Sep. 2015.

[25] D. Ounnas, S. Chenikher, and T. Bouktir, "Tracking control for permanent magnet synchronous machine based on Takagi–Sugeno fuzzy models," in *Proc. IEEE Ecological Veh. Renewable Energies*, 2013, pp. 1–5.

Yuan-Chih Chang (M'12) was born in Taiwan, on April 23, 1978. He received the B.S. degree in electrical engineering from National Taiwan University, Taipei, Taiwan, in 2002, and the Ph.D. degree in electrical engineering from National Tsing Hua University, Hsinchu, Taiwan, in 2009.

In 2009, he was with the faculty of the Department of Electrical Engineering, National Chung Cheng University, as an Assistant Professor. He is currently an Assistant Professor at National Chung Cheng University, Taiwan. His research interests include power electronics, motor drives, generator drive system, and electric machine control.

Chien-Hua Chen was born in Taiwan, on December 2, 1991. He received the B.S. degree in electrical engineering from Chung Yuan Christian University, Taoyuan, Taiwan, in 2014. He is currently working toward the Graduate degree at National Chung Cheng University, Chiayi, Taiwan.

His research interests include power electronics, permanent-magnet synchronous generator, and motor drives.

Zhong-Chuan Zhu was born in Taiwan, on January 21, 1991. He received the B.S. degree in electrical engineering from the National Chin-Yi University of Technology, Taichung, Taiwan, in 2013, and the Master's degree in electrical engineering from National Chung Cheng University, Chiayi, Taiwan, in 2015.

He is currently working with Delta Electronics Inc., Tainan, Taiwan. His research interests include permanent-magnet synchronous motor drives and fuzzy controls.

Yi-Wen Huang was born in Taiwan, on September 5, 1991. She received the B.S. degree in electrical engineering from National Formosa University, Yunlin, Taiwan, in 2014. She is currently working toward the Graduate degree at National Chung Cheng University, Chiayi, Taiwan.

Her research interests include wind energy generation systems and power electronics.